Backwards and forwards relative dispersion in turbulent flow: An experimental investigation

Jacob Berg,* Beat Lüthi, Jakob Mann, and Søren Ott
Risø National Laboratory, 4000 Roskilde, Denmark
(Received 3 January 2006; revised manuscript received 23 May 2006; published 27 July 2006)

From particle tracking velocimetry we present an experimental measure of the ratio between backwards and forwards relative dispersion in an intermediate Reynolds number turbulent flow. Lack of time-reversal symmetry implies that their ratio may be different from 1. From a stochastic model, this has recently been studied by Sawford *et al.* [Phys. Fluids **17**, 095109 (2005)] giving ratios between 5 and 20. We find a value of approximately 2 and discuss it in the context of the characteristics of the rate of strain tensor s_{ij}. An analysis of a direct numerical simulation by Biferale *et al.* [Phys. Rev. Lett. **93**, 064502 (2004) and Phys. Fluids **17**, 021701 (2004)] gives the same result.

DOI: 10.1103/PhysRevE.74.016304 PACS number(s): 47.27.tb, 47.27.Gs

I. INTRODUCTION

Turbulence is the state of fluid flow far from its equilibrium laminar state. It is governed by the Navier-Stokes equation and is highly nonlinear. Although there have been many attempts, Kolmogorov's four-fifths law [1] is still the only result derived rigorously from the Navier-Stokes equation. An important aspect of turbulence is its ability to efficiently transport and mix matter, heat, and momentum. Relative dispersion describes the separation in time of nearby fluid particles. Transport and mixing properties in turbulent flow are therefore associated with this phenomenon.

Richardson [2] was the first to analyze relative dispersion. He linked the problem to a diffusion equation and empirically derived a scale-dependent eddy diffusivity of a cloud of fluid elements. Obukhov [3] later refined the theory relating the mean-square separation of an initially close pair of fluid elements to the kinetic energy dissipation ε of the flow,

$$\langle r^2 \rangle = g \varepsilon t^3. \tag{1}$$

The Richardson law expressed in Eq. (1) is supposed to be valid in the inertial range where influences from the large-scale forcing and small-scale viscous effects can be neglected. The Richardson-Obukhov constant g seems to be a function of Reynolds number Re_λ presumably with an asymptotic limit at high Reynolds number [4].

The Lagrangian nature of turbulent pair separation makes computational and experimental tests very difficult since a large separation of temporal scales is needed. Yeung [5] concluded based on extrapolations from low Re_λ direct numerical simulation (DNS) data that at least $\mathrm{Re}_\lambda \sim 600-700$ is needed. Previous studies at moderate Re_λ [6–9] have, however, succeeded in providing insight into the Richardson law, although a definitive scaling has hardly been observed.

A striking feature of hydrodynamical turbulence compared to a Gaussian flow is the existence of nonzero odd moments of the distributions of velocity differences: the structure functions. The four-fifths law is the most well known example of this. It implies that time reversibility breaks down in the inertial range.

A consequence is that if you follow the separation of two fluid elements forward in time, then follow the same two particles backward in time, the latter separation will occur at a different speed. In mixing applications this could play a significant role.

Calculating the future width of a puff released at time $t=0$ is a classical forwards dispersion problem. If, on the other hand, one wants to calculate the fluctuations in some scalar concentration at some time t, one will have to follow the particles backwards in time: the different trajectories carry different scalar concentrations from the past.

This forward/backward asymmetry was, however, only recently emphasized by Sawford *et al.* [10]. They noticed that both processes can be described with the Richardson law with different values of the constant g. They investigated two different Lagrangian stochastic models for relative dispersion in the inertial range and concluded that the process of backwards dispersion was much faster than the corresponding forward case. This has implications for practical calculations of turbulent mixing, such as, for example, combustion and pollution.

On an experimental level, no evidence of the asymmetry has been reported. In this paper, we will present an analysis of an intermediate Reynolds number flow. Sawford *et al.* [10] noticed the high computational costs for studying DNS data. We have, however, come up with an *easy to do* scheme that avoid this computational problem. DNS data will therefore be analyzed and compared with our experimental findings.

Determining the ratio between the backwards and forwards dispersion defined as g_b/g_f, where g_b and g_f refer to the Richardson-Obukhov constants for the backward and forward case, respectively, is the objective of the present paper.

Sections II and III will go through the technique of particle tracking velocimetry and characterize the experimental flow. In Sec. IV, we will present the results after a short discussion of how to obtain dispersion results in a finite Reynolds number flow. The section will end with a short presentation of DNS data analyzed in the same way as the experimental data. In the Discussion section, we will present some heuristic arguments relating the difference between forwards and backwards relative dispersion to the mechanism of infinitesimal material line stretching taking place in the viscous range. Section VI will conclude with our findings.

*Electronic address: jacob.berg.joergensen@risoe.dk

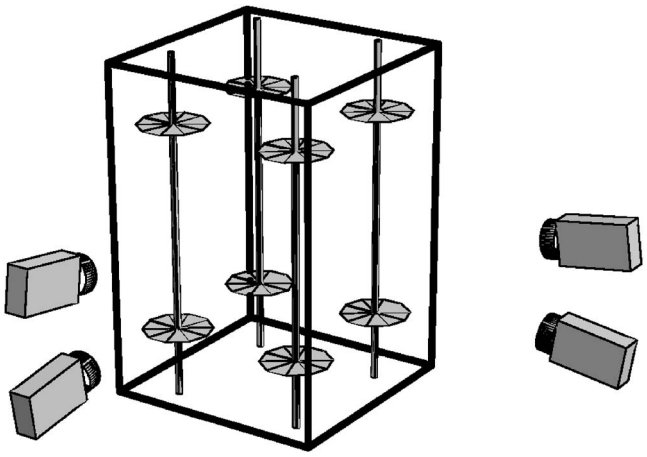

FIG. 1. Experimental setup.

II. EXPERIMENTAL METHOD

We have performed a particle tracking velocimetry (PTV) experiment in an intermediate Reynolds number turbulent flow. Lagrangian trajectories of fluid elements in water are obtained by tracking neutrally buoyant particles in space and time. The flow is generated by eight rotating propellers (which change their rotational direction in fixed intervals) placed in the corners of a tank with dimensions $32\times32\times50$ cm^3 (see Fig. 1).

The data acquisition system consists of four commercial CCD cameras with a maximum frame rate of 50 Hz at 1000×1000 pixels. Two different setups are used. The first covers a measuring volume of roughly $(12\text{ cm})^3$. Here we use polystyrene particles with size ~400 μm and density very close to 1. We follow $O(1000)$ particles at each time step with a position accuracy of 0.05 pixels corresponding to less than 10 μm. Due to the large particle size and separation, we cannot study viscous effects in this setup. We therefore also use micro tracking where the volume is only $(1\text{ cm})^3$ in order for the viscous scales to be resolved. In this setup, we use cenosphere particles with size ~100 μm.

In both setups, the Stokes number, τ_I/τ_η (τ_I denotes the inertial relaxation time for the particle to the flow while τ_η is the Kolmogorov time), is much less than 1 and the particles can therefore be treated as passive tracers in the flow. The particles are illuminated by a 250 W stroboscope.

The large volume (macro tracking settings) is used for the main results presented in Sec. IV while the small volume (micro tracking settings) is used only for the heuristic arguments presented in the Discussion section.

The mathematical algorithms for translating two-dimensional (2D) image coordinates from the four camera chips into a full set of three-dimensional (3D) trajectories in time involve several crucial steps: fitting Gaussian profiles to the 2*D* images, stereo matching (line of sight crossings) with a two-media (water-air) optical model, and construction of 3D trajectories in time by using the kinematic principle of minimum change in acceleration [11,12].

III. FLOW PROPERTIES

We study a particular flow at intermediate Reynolds number in the large volume (macro tracking settings). Figure 2 shows the standard deviations of the three velocity components: the two horizontal (radial) $\sigma_{u_x},\sigma_{u_y}$ and the vertical (axisymmetric) σ_{u_z}. The figure shows the standard deviations averaged over three different planes: *yz* plane, *xz* plane [both in panel (a)], and *xy* plane [in panel (b)]. In both panels the two horizontal components are observed to collapse on values around 22 mm/s with almost no dependence on the vertical or the horizontal positions. The vertical component has a dependence on the vertical coordinate z with a minimum $\sigma_{u_z}=15.1$ mm/s at $z=18$ mm indicating the symmetry plane of the flow.

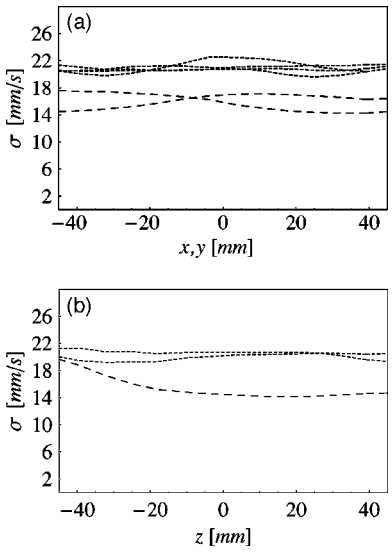

FIG. 2. (a) Standard deviations of the velocity components averaged over the *yz* plane and the *xz* plane. The dotted lines correspond to the radial components while the dashed lines correspond to the axisymmetric vertical component. (b) Same as in (a) but averaged over the *xy* plane.

The turbulence characteristics are given in Table I. The values have been obtained by fitting a von Kármán model to the experimental obtained longitudinal second-order structure function $f(r)\equiv\langle\delta v_\parallel^2(r)\rangle$ [6]. The model fit is shown in Fig. 3(a). The method determines ε with a 10% error. In computing $f(r)$ from data, the averages were taken over all separations $\mathbf{r}$ with $|\mathbf{r}|=r$ within a ball fully inside the measuring volume.

We have measured the normal component of the longitudinal mean acceleration

TABLE I. Macro tracking turbulence characteristics obtained from fits to the von Kármán model. ε is the mean kinetic energy dissipation; $\eta\equiv(\nu^3/\varepsilon)^{1/4}$ is the Kolmogorov length scale with the kinematic viscosity ν of water. $\tau_\eta\equiv(\nu/\varepsilon)^{1/2}$ is the Kolmogorov time scale. The integral length scale is L_{int} while T_L is the integral time scale. $\sigma_u^2=\frac{1}{3}(\sigma_{u_x}^2+\sigma_{u_y}^2+\sigma_{u_z}^2)$ is the standard deviation of velocity. The Reynolds number is defined as $\text{Re}_\lambda=\frac{\lambda\sigma_u}{\nu}$ with the Taylor micro scale $\lambda=\sqrt{\left(\frac{15\nu\sigma^2}{\varepsilon}\right)}$.

η	L_{int}	τ_η	T_L	ε	σ_u	Re_λ
0.25 mm	48 mm	0.07 s	2.45 s	168 mm^2/s^3	23.33 mm/s	172

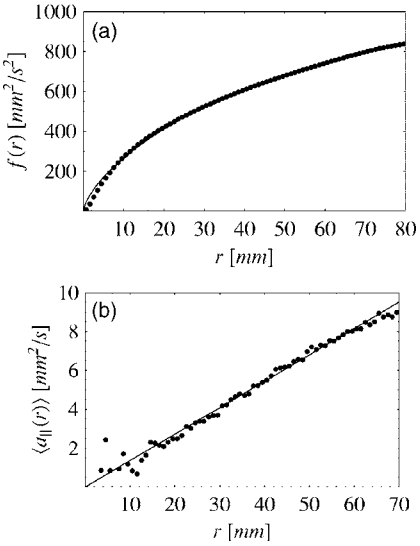

FIG. 3. (a) $f(r)$ with the fitted von Kármán model on top (full line). (b) $\langle \delta a_{\|}(r)\rangle$ with a linear fit.

$$\langle \delta a_{\|}(r)\rangle \equiv \left\langle \delta \mathbf{a}(r) \cdot \frac{\mathbf{r}}{r} \right\rangle \tag{2}$$

between two points separated a distance r. In a globally homogeneous flow, this quantity is zero for all values of r and the second-order structure of the turbulence can be solely described by a single function, namely $f(r)$ [6]. Most real flows are, however, not globally homogeneous and therefore a net mean acceleration may exist. $\langle \delta a_{\|}(r)\rangle$ is plotted in Fig. 3(b). The acceleration is observed to increase linearly. The solid straight line is a linear fit of the form $y(r)=\alpha r+\beta$. Here $\alpha=0.13$ mm/s and β is very close to zero. From the axisymmetric properties of the flow we expect the mean acceleration to be of the form $\delta u^2/r$ so that

$$\alpha r = \langle \delta a_{\|}(r)\rangle = u^2 \quad \Rightarrow \tag{3}$$

$$\phi = \frac{\sqrt{\alpha}}{2\pi} = 0.057 \text{ s}^{-1}, \tag{4}$$

where ϕ is the frequency. Because $\alpha>0$, the flow is straining (in contrast to a full body rotation with $\delta a<0$). Taking the reciprocal of ϕ gives us a characteristic time scale for the straining motion of the order 18 s. This number is much larger than the integral time scale T_L, therefore we do not expect any significant influence of the mean flow on the results presented later.

IV. RESULTS

Recently, Bourgoin *et al.* [13] performed a PTV experiment at $\mathrm{Re}_\lambda \sim 800$. Besides being the PTV experiment with the largest Re_λ so far, it is the first study to shed light on the small time expansion and acknowledge its great importance on relative separation of particles in turbulent flow.

They find a very robust ballistic regime (the mean-square separation is proportional to t^2) for times smaller than the Batchelor time $t_0=(r_0^2/\varepsilon)^{1/3}$. This is the time for which particle pairs are strongly influenced by their initial separation r_0 and can fully be described by the second-order Eulerian structure function. The Richardson law is only valid for times much larger than t_0 and should therefore be independent of initial separations, as long as they are small but still larger than the Kolmogorov scale. It is therefore an asymptotic relation that is approached at infinite Re_λ.

At finite Re_λ we have a relation of the general form

$$\langle r^2\rangle/r_0^2 = \mathcal{F}(t/t_0, \eta/r_0, \mathrm{Re}_\lambda), \tag{5}$$

where we have chosen r_0 and t_0 as scales to make the relation dimensionless. For a given Re_λ the inertial range is found where $t/t_0 \ll T_L/t_0 \propto (\eta/r_0)^{2/3}\mathrm{Re}_\lambda$ and $\eta/r_0 \approx 0$. In the inertial range, therefore, we have

$$\langle r^2\rangle/r_0^2 = \mathcal{F}(t/t_0, 0, \mathrm{Re}_\lambda). \tag{6}$$

We can now, without loss of generality, express $\mathcal{F}$ in terms of the two functions Φ and Θ,

$$\mathcal{F}(t/t_0, 0, \mathrm{Re}_\lambda) \equiv \Phi(t/t_0, \mathrm{Re}_\lambda)[t/t_0 - \Theta(\mathrm{Re}_\lambda)]^3. \tag{7}$$

If there is an asymptotic law for $\mathrm{Re}_\lambda \to \infty$, then $\Theta(\mathrm{Re}_\lambda)$ must approach a constant value and $\Phi(t/t_0, R_\lambda)$ must approach a function $\Phi(t/t_0, \infty)$ in that limit. Substituting $t_0=r_0^{2/3}\varepsilon^{-1/3}$ and letting $\mathrm{Re}_\lambda \to \infty$, we can rewrite the relation as

$$\langle r^2\rangle = \Phi(t\varepsilon^{1/3}r_0^{-2/3}, \infty)\varepsilon[t - r_0^{2/3}\varepsilon^{-1/3}\Theta(\infty)]^3. \tag{8}$$

If we let $r_0 \to 0$, then we arrive at the Richardson law *provided* that $\Phi(x, \infty)$ approaches a constant value $\Phi(\infty, \infty) \equiv g$ as $x \to \infty$, where g is the Richardson-Obukhov constant. This means, on the other hand, that keeping r_0 finite but letting $t \to \infty$ leads to the relation

$$\langle r^2\rangle = \Phi(\infty, \infty)\varepsilon[t - r_0^{2/3}\varepsilon^{-1/3}\Theta(\infty)]^3. \tag{9}$$

Denoting $\Theta(\mathrm{Re}_\lambda)$ T_0, we finally arrive at the finite Reynolds number expression as introduced by Ott and Mann [6],

$$\langle r^2(t)\rangle/r_0^2 = g(t/t_0 - T_0/t_0)^3. \tag{10}$$

When r_0 is in the inertial range, the only available time scale is t_0 so that $T_0=st_0$, where s is independent of r_0. The time shift T_0 is thus a result of processes taking place in the initial phase. When these processes have ceased, and the dispersion has lost its memory of them, the time shift is the only thing that remains—it cannot be removed by any mechanism.

The mixing of viscous and long-range effects in finite Reynolds number turbulence motivated Biferale *et al.* [9] to study exit times. The method is very promising, although it is not possible to determine the Richardson-Obukhov constant without a model for relative separation.

A. PTV

We do not expect to find any significant Richardson-Obukhov scaling. The finiteness of the Reynolds number and of the observational domain are to be held responsible for this. For the latter part: the main effect would be a bias toward lower exponents of t: rapidly separating particles may

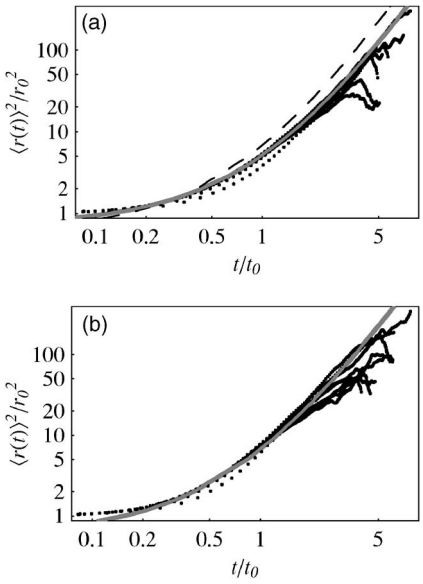

FIG. 4. (a) $\langle r^2(t)\rangle/r_0^2$ as a function of t/t_0 in the forward case. The different dotted lines correspond to different initial separations r_0 from $4-8\,\eta$ to $24-28\,\eta$. A fit to data by Eq. (10) is plotted as the gray solid line. The dashed line is the backward case fit. (b) Backward case.

leave the volume making $\langle r^2(t)\rangle$ smaller than it would have been in an infinite volume. We have tried to reduce this effect by using an observational volume several times the size of the integral length scale as well as only used pairs that start within a small subvolume ($r=30$ mm) of the full observational domain.

We look at particles that start within bins of size $4\,\eta$ corresponding to one millimeter. The largest bin is $24-28\,\eta$ while the smallest is $4-8\,\eta$. In order to make the selection of pairs independent from the previous time step, we define a new pair each time two arbitrarily chosen particles come within the bin size of the initial separation r_0. In this way, the same two particles can contribute to the ensemble many times.

Figure 4 shows $\langle r^2(t)\rangle/r_0^2$ as a function of t/t_0 in the backward and forward case. All bins are included in the two plots. A fit to the data by Eq. (10) is also shown. From around $t\sim 0.2t_0$ the fits agree with data. One curve is, however, observed to fall below the other curves. This is the smallest bin that is not expected to be in the inertial range. For times smaller than $t\sim 0.2t_0$, the separation is not in the inertial range and Eq. (10) is therefore not valid. For large times, all the curves are observed to *drop down*. It happens earlier for curves corresponding to larger bins. This is due to the narrow inertial range as well as finite volume effects, as discussed earlier.

From fits to Eq. (10) we obtain g values of $g_f=0.55\pm0.05$ and $g_b=1.15\pm0.05$ for the forward and backward case, respectively. The error is the rms value for the different r_0. No systematic dependence was found.

The forward value g_f is similar to values obtained from both DNS and experiments [6–9] at different Reynolds numbers. Franzese and Cassiani [4] derive g_f as a function of Reynolds number which saturates slightly above 0.6 for

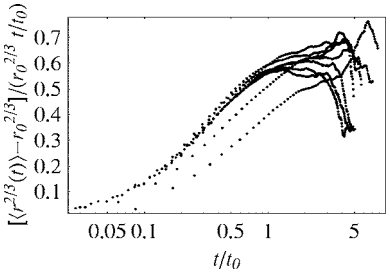

FIG. 5. $(\langle r^{2/3}\rangle - r_0^{2/3})/(r_0^{2/3}t/t_0)$ vs t/t_0. The different curves correspond to the different bins.

$\mathrm{Re}_\lambda\sim 350$. Between $\mathrm{Re}_\lambda\sim 150$ and higher, the function is only very weakly dependent on Re_λ.

The ratio g_b/g_f is 2.09, making it significantly smaller than the ratios found by Sawford *et al.* [10]. Depending on parameter choices in their stochastic models, they predict $g_b/g_f\sim 5-20$. The fact that our inertial range is narrow and that the stochastic models are based on K41 inertial range, scaling arguments might explain some of the discrepancy.

The time shift T_0 in Eq. (10) is $T_0^f=(1.12\pm0.02)t_0$ and $T_0^b=(0.80\pm0.02)t_0$. As expected, it is the same order of magnitude as t_0. Another way of arriving at the result just presented would be to follow the original lines by Ott and Mann [6], where T_0 is obtained as the zero crossing of $\langle r^2(t)\rangle^{1/3}$ with the time axis.

The excellent fit for both backwards and forwards dispersion presented in Fig. 4 supports the existence of the inertial range universal function $\mathcal{F}$ defined in Eq. (6). In our experiment, $\mathcal{F}$ is valid over a decade of t/t_0. We do not claim that we have observed true Richardson scaling. This would mean that all curves representing different bins would collapse on a single straight line in a log-log coordinate system of r versus t with slope 3 (not shown). A very large Reynolds number together with a large observational volume many times the integral scale would be necessary to observe such a regime. The clear difference between the forward and backward case that we observe is, on the other hand, a clear indication that the dynamics is much more complex than purely ballistic motion where forward and backward dispersion are the same.

Bourgoin *et al.* [13] suggested that the inequality $T_L/t_0>10$ should be fulfilled in order to observe any Richardson-like behavior. They arrive at this inequality by plotting the quantity $(\langle r^{2/3}\rangle - r_0^{2/3})/(r_0^{2/3}t/t_0)$ versus t/t_0 and looking for plateaus. Only for the smallest initial separation for which T_L/t_0 is of order 10 do they observe a transition to a plateau. For comparison (Fig. 4 in their paper) we have plotted the same quantity for the forward dispersion case in our experiment. Figure 5 show the curves for the different bins. Except for the two smallest bins, plateaus are observed at $t\sim t_0$ for all bins. Important in this context is that $T_L/t_0<10$ for all bins in our experiment.

A few differences in the two experiments might explain the difference in T_L/t_0 and the transition to a Richardson-like behavior observed in Fig. 5: r_0/η and $L_{\mathrm{vol}}/L_{\mathrm{int}}$, where L_{vol} is the diameter of the observation volume. In the experiment by Bourgoin *et al.*, $L_{\mathrm{vol}}/L_{\mathrm{int}}\sim 1$ and $r_0/\eta\in\{43;2150\}$. In our experiment, $L_{\mathrm{vol}}/L_{\mathrm{int}}\sim 2.5$ and $r_0/\eta\in\{4;28\}$. $L_{\mathrm{vol}}/L_{\mathrm{int}}$ is a

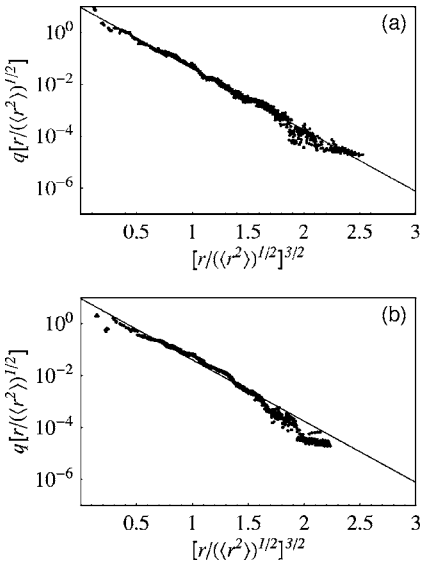

FIG. 6. (a) Distance-neighbor function for forward dispersion for pairs starting at $8-12\eta$, (b) backward case. In both plots, the straight line is the prediction by Richardson.

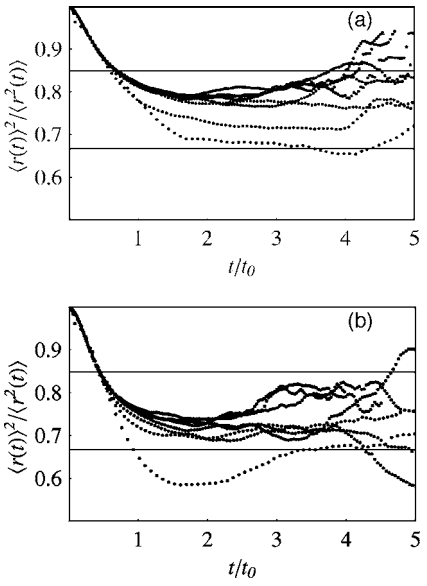

FIG. 7. (a) $\langle r(t)\rangle^2/\langle r^2(t)\rangle$ as a function of t/t_0 for the forward case. The different lines correspond to different initial separations: r_0 increasing upward from $r_0=4\eta$ to $r_0=28\eta$ in bins of 4η. The horizontal lines are the Richardson prediction at 0.67 and the Gaussian prediction at 0.85. (b) Backward case.

measure of possible finite volume bias whereas the implications of r_0/η are more subtle. Bourgoin *et al.* explore a wide range of initial separations where at least the smallest ones lie fully and unambiguously in the inertial range. Our Reynolds number is significantly lower and it is therefore not possible for us to explore the same range of initial separations in the inertial range. Because our ratios of r_0/η are smaller, we can follow particle pairs for longer times—both physical time as well as in time rescaled with t_0. An objection toward our relative low ratio of r_0/η would be that none of the separations lie fully in the inertial range. However, we defined the inertial range universal function $\mathcal{F}$ based on the argument that $\eta/r_0 \sim 0$. So for the validity of $\mathcal{F}$, the ratio r_0/η is not too low.

To quantify how far away we are from a fully developed Richardson regime, we will now look at the probability density function (pdf) of separation: the Richardson distance-neighbor function $q(r)$ is the solution to a diffusion equation with scale-dependent diffusivity $K(r) \sim r^{4/3}$ [6].

The data are plotted in Fig. 6 for initial separations between 12η and 16η. The Richardson prediction is shown as a straight line. In both case, excellent agreement is observed.

If, however, we look at the moments of the pdf, we observe that the Richardson prediction may not be the best description for the experimental data: the ratio between the first two moments of the pdf's is displayed in Fig. 7. Besides the smallest initial separations ($r_0=4\eta$ and 8η, which are probably not even in the inertial range), the curves almost collapse. The scatter observed for long times is due to poor statistics and should not be subject to any physical interpretation. Although the backward case seems to be closer to the Richardson value (the bottom most horizontal line), both cases are certainly not Gaussian (topmost horizontal line).

B. DNS

In addition to the experimental findings, we have performed a similar analysis on direct numerical simulation data (DNS). Details about the simulation can be found in Biferale *et al.* [14,15].

We have again sorted r_0 in bins of size 4η. This approach is somewhat different from the usual DNS approach, where r_0 is a finite number and not, as here, an interval. Doing it our way we can, however, get information on the backwards dispersion from databases of only tracks, without having to store the full Eulerian velocity field in time [10]. The DNS simulates the three-dimensional Navier-Stokes equations at a resolution of 1024^3 corresponding to $\mathrm{Re}_\lambda \sim 280$. In nondimensional units, $\varepsilon=0.81$, $\nu=8.8\times10^{-4}$, $\eta=5\times10^{-3}$, and $L=3.14$ with Lagrangian velocity autocorrelation time and Kolmogorov time, $T_L=1.2$ and $\tau=3.3\times10^{-2}$, respectively.

We plot $\langle r^2(t)\rangle/r_0^2$ as a function of t/t_0 in Fig. 8 for both forwards and backwards dispersion for the case $r_0=20\eta$. The dashed lines are fits to Eq. (10). After a time $t \sim t_0$, the fits are in excellent agreement with the data. Figure 9 reveals a small dependence of g_f, g_b, and g_b/g_f on r_0/η. g_b/g_f decreases from 2.4 to 2.2 with increasing r_0/η. The fact that the smallest initial separations are not in the inertial range may explain this behavior.

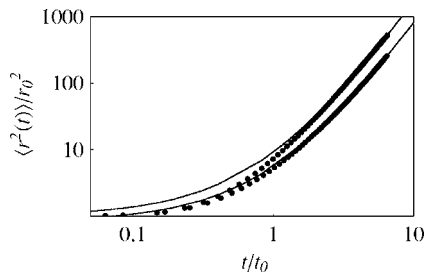

FIG. 8. $\langle r^2(t)\rangle/r_0^2$ as a function of t/t_0 for the two cases with $r_0=20\eta$. Fits by Eq. (10) are displayed on top by thin lines. The upper curve is the backward case.

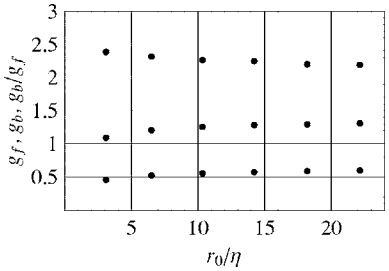

FIG. 9. g_f, g_b, and g_b/g_f (from bottom to top) as a function of r_0/η.

It is noteworthy that $g_b/g_f \sim 2$ as in the experiment, although the general flow properties of the DNS and experimental flow are different: whereas the experimental flow is axisymmetric and slightly strained, the DNS is isotropic. In DNS, the forcing on the smallest wave numbers in Fourier space gives rise to a vanishing $\langle \delta a_{\|}(r) \rangle$.

Along with these differences between the experiment and the DNS, there are other physical differences of importance. The first and probably most striking is the Lagrangian nonstationarity [16]. In the experiment, a fluid particle will experience a decrease in kinetic energy with time as it moves away from the forcing propellers. From time to time it will, however, due to the finite volume, come back to the propellers once again and gain kinetic energy. In agreement with decaying turbulence, $\frac{d}{dt}\langle u^2 \rangle = -\varepsilon$. In DNS, in contrast, we have that $\frac{d}{dt}\langle u^2 \rangle = 0$.

Another difference is the number of integral time scales observed. Whereas the DNS only has $\sim 3.7 T_L$, the experiment has $\sim 154 T_L$. The volume size in terms of integral scale is similar to our experiment ($L_{\mathrm{vol}}/L_{\mathrm{int}}=2$).

The close agreement between g_b/g_b in the experiment and in the DNS data indicates that the result is robust and, perhaps more importantly, that DNS can in a satisfactory way be used to simulate turbulence in the absence of real physical experiments.

V. DISCUSSION

The difference between forwards and backwards dispersion can be explained in part in terms of stretching of infinitesimal material line elements l. These obey the kinematic relation

$$\frac{1}{2}\frac{Dl^2}{Dt} = l_i l_j s_{ij} \tag{11}$$

with the rate of strain tensor, $s_{ij} = \frac{1}{2}\left(\frac{\partial u_i}{\partial x_j} + \frac{\partial u_j}{\partial x_i}\right)$. The eigenvalues of s_{ij}, Λ_i are defined such that $\Lambda_1 > \Lambda_2 > \Lambda_3$, and $\Sigma_i \Lambda_i = 0$ due to incompressibility. Batchelor [17] proposed that any infinitesimal material line element will, after a short time, align itself with the largest eigenvalue and therefore $\frac{1}{2}Dl^2/Dt = \Lambda_1 l^2$.

From our experimental micro tracking, we can calculate the distributions of Λ_i in a flow with $\mathrm{Re}_\lambda \sim 100$. An ansatz for the linearity of the velocity field in the proximity of the particle positions is used to obtain the eigenvalues, Λ_i. Details of the method can be found in Lüthi *et al.* [18].

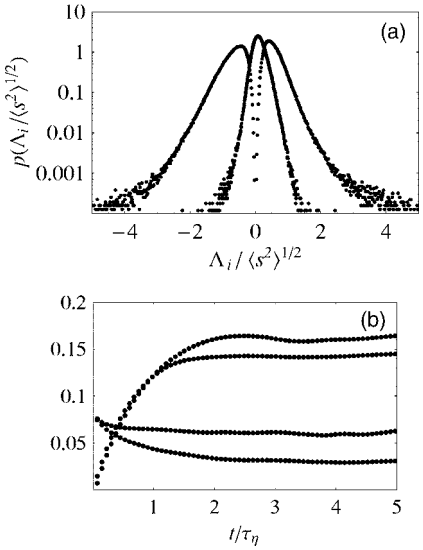

FIG. 10. (a) PDF of Λ_i. The PDFs are normalized with the rms of total strain $\langle s^2 \rangle^{1/2}$. (b) Stretching rates as a function of time. From bottom to top: var($L_f(t)$), var($L_b(t)$), $\langle L_f(t) \rangle$, and $\langle L_b(t) \rangle$.

Figure 10(a) shows the distributions of Λ_i. We find the ratio

$$\langle \Lambda_1^f \rangle : \langle \Lambda_2^f \rangle : \langle \Lambda_3^f \rangle = 1.00 : 0.20 : -1.20.$$

Other experiments found similar values: Kholmyansky *et al.* [19] in an atmospheric flow at $\mathrm{Re}_\lambda = 10^4$ and Lüthi *et al.* [18] in a magnetically forced flow at $\mathrm{Re}_\lambda = 50$. Betchov [20] calls it the jet collision situation: compression of material lines in one direction and stretching in the other two directions. We can associate this situation with forward infinitesimal separation of fluid particles. In the backward case, we simply change the sign of all three eigenvalues resulting in

$$\langle \Lambda_1^b \rangle : \langle \Lambda_2^b \rangle : \langle \Lambda_3^b \rangle = -1.00 : -0.20 : 1.20.$$

Recent studies [21–23] indicate that coarse-grained strain dynamics are similar to their viscous counterpart. More importantly, it seems that even the eigenvalues are very similar to the ones found in coarse-grained fields by Borue and Orszag [23]. The above picture may thus be extended to scales, $l > \eta$, and hence into the inertial range. In order to connect the theory for infinitesimal material line stretching to inertial range dispersion, we therefore assume self-similarity of material line stretching.

Based on the above assumptions, we can estimate the ratio, g_b/g_f. The characteristic time of separation is determined by the largest mean eigenvalue: $\langle \Lambda_1 \rangle$ and $-\langle \Lambda_3 \rangle$ for the forward and backward case, respectively. In the forward case where $t > 0$, we recall $\langle r^2(t) \rangle_f = g_f \varepsilon t^3$. Looking now at $t < 0$ with normalized time, we have

$$\langle r^2(t) \rangle_b = \left\langle r^2\left(t\frac{-\langle \Lambda_3 \rangle}{\langle \Lambda_1 \rangle}\right)\right\rangle_f = g_f \varepsilon \left(t\frac{-\langle \Lambda_3 \rangle}{\langle \Lambda_1 \rangle}\right)^3 = g_b \varepsilon t^3,$$

which means that

$$g_b/g_f = \left(\frac{\langle -\Lambda_3\rangle}{\langle \Lambda_1\rangle}\right)^3 = 1.75. \quad (12)$$

This value is within the errors of the value found earlier, even though the $\langle\Lambda_i\rangle$ was obtained from the viscous range and the relative dispersion experiment was performed in the inertial range.

The picture is, however, more complicated. To illustrate this, we compute the stretching rate $L(t)$ defined as $L(t)/\tau_\eta \equiv \frac{1}{2}l^{-2}Dl^2/Dt$ from Eq. (11). For large times, we expect $L(t)$ to reach a steady state that can be associated with the Lyapunov exponent defined as $\lambda = \lim_{t\to\infty}\langle L(t)\rangle$ [7,9]. The computation of the two cases only differs by a sign change in the time integration. $\langle L(t)\rangle$ and the variance var$(L(t))$ for both cases are shown in Fig. 10(b). Both the asymptotic λ and its variance are highest in the backward case. $\lambda_f = 0.145$ is similar to values found by others: 0.115 ± 0.005 [9] and 0.129–1.400 [24].

Comparing λ_f and λ_b with the actual largest mean eigenvalue, $\langle\Lambda_1\rangle$ in the forward case and $-\langle\Lambda_3\rangle$ in the backward case, we see that the values obtained are around 40% of the eigenvalues. This is of course reflecting the known fact that the material line elements are far from being perfectly aligned with the largest eigenvalue as proposed by Batchelor [24–26]. This is a first indication that the picture of calculating the ratio g_b/g_f from $\langle\Lambda_1\rangle$ and $\langle\Lambda_3\rangle$ alone is far too simplistic. More severe, though, is the assumption of self-similarity of material line stretching, which implies that particle separation vectors align with the coarse-grained principal strain field. Future experimental investigations will focus on this last issue.

VI. CONCLUSION

A PTV experiment in a turbulent flow has been performed. Because our Reynolds number is only of intermediate size, we do not observe a fully developed Richardson regime. We therefore propose a function $\mathcal{F}$ of particle pair separation that take into account the effect of initial separation. We show experimental evidence of the existence of this function. It is hereafter utilized to quantify dispersion rates.

The experiment showed a difference between forwards and backwards dispersion. The mean square separation following particle pairs backwards in time is twice as large as forwards. DNS data support this finding, indicating that the result is robust to forcing and Lagrangian stationarity.

Whereas Sawford *et al.* [10] focused on the role of the odd moments to explain the difference between forwards and backwards dispersion, we suggest alternatively that the positiveness of $\langle\Lambda_2\rangle$ might explain the faster backwards dispersion as compared to the corresponding forwards dispersion.

ACKNOWLEDGMENTS

We thank the supercomputing center Cineca (Bologna, Italy) for the hosting of the DNS data. This work was supported by the Danish Technical Research Council under Contract No. 26-01-0087.

[1] U. Frisch, *Turbulence* (Cambridge University Press, Cambridge, 1995).
[2] L. F. Richardson, Proc. R. Soc. London, Ser. A **110**, 709 (1926).
[3] A. M. Obukhov, Izv. Akad. Nauk SSSR, Ser. Fiz. **5**, 453 (1941).
[4] P. Franzese and M. Cassiani (unpublished).
[5] P. K. Yeung, Annu. Rev. Fluid Mech. **34**, 115 (2002).
[6] S. Ott and J. Mann, J. Fluid Mech. **422**, 207 (2000).
[7] G. Boffetta and I. M. Sokolov, Phys. Fluids **6**, 094501 (2002).
[8] T. Ishihara and Y. Kaneda, Phys. Fluids **14**, L69 (2002).
[9] L. Biferale, G. Boffetta, A. Celani, B. J. Devenish, A. Lanotte, and F. Toschi, Phys. Fluids **17**, 115101 (2005).
[10] B. L. Sawford, P. K. Yeung, and M. S. Borgas, Phys. Fluids **17**, 095109 (2005).
[11] J. Willneff, Ph.D. thesis, ETH, Zürich (2003).
[12] N. T. Ouellette, H. Xu, and E. Bodenschatz, Exp. Fluids **40**, 301 (2006).
[13] M. Bourgoin, N. T. Ouellette, H. Xu, J. Berg, and E. Bodenschatz, Science **311**, 835 (2006).
[14] L. Biferale, G. Boffetta, A. Celani, B. J. Devenish, A. Lanotte, and F. Toschi, Phys. Rev. Lett. **93**, 064502 (2004).
[15] L. Biferale, G. Boffetta, A. Celani, B. J. Devenish, A. Lanotte, and F. Toschi, Phys. Fluids **17**, 021701 (2005).
[16] S. Ott and J. Mann, New J. Phys. **7**, 142 (2005).
[17] G. K. Batchelor, Proc. R. Soc. London, Ser. A **213**, 349 (1952).
[18] B. Lüthi, A. Tsinober, and W. Kinzelbach, J. Fluid Mech. **528**, 87 (2005).
[19] M. Kholmyansky, A. Tsinober, and S. Yorish, Phys. Fluids **13**, 311 (2001).
[20] R. Betchov, J. Fluid Mech. **1**, 497 (1956).
[21] B. Tao, J. Katz, and C. Meneveau, J. Fluid Mech. **457**, 35 (2002).
[22] F. van der Bos, B. Tao, and J. K. C. Meneveau, Phys. Fluids **14**, 2456 (2002).
[23] V. Borue and S. A. Orszag, J. Fluid Mech. **366**, 1 (2002).
[24] S. S. Girimaji and S. B. Pope, J. Fluid Mech. **220**, 427 (1990).
[25] A. Tsinober, *An Informal Introduction to Turbulence* (Kluwer, Dordrecht, 2001).
[26] M. Guala, B. Lüthi, A. Liberzon, A. Tsinober, and W. Kinzelbach, J. Fluid Mech. **533**, 339 (2005).